Nucleophilic Substitution in Reactions between Partially Hydrated Superoxide Anions and Alkyl Halides

ARTICLE *in* THE JOURNAL OF ORGANIC CHEMISTRY · JUNE 2015

Impact Factor: 4.72 · DOI: 10.1021/acs.joc.5b00651 · Source: PubMed

4 AUTHORS:

Mauritz Ryding

University of Oslo

15 PUBLICATIONS **86** CITATIONS

SEE PROFILE

Andrea Debnárová

University of Oslo

10 PUBLICATIONS **48** CITATIONS

SEE PROFILE

Israel Fernández

Complutense University of Madrid

188 PUBLICATIONS **3,054** CITATIONS

SEE PROFILE

Einar Uggerud

Royal Adelaide Hospital

155 PUBLICATIONS **2,013** CITATIONS

SEE PROFILE

JOC The Journal of Organic Chemistry

Article

pubs.acs.org/joc

Nucleophilic Substitution in Reactions between Partially Hydrated Superoxide Anions and Alkyl Halides

Mauritz J. Ryding,*[,†] Andrea Debnárová,[†] Israel Fernández,[‡] and Einar Uggerud*[,†]

[†]Mass Spectrometry Laboratory and Centre of Theoretical and Computational Chemistry, Department of Chemistry, University of Oslo, P.O. Box 1033 Blindern, NO-0315 Oslo, Norway

[‡]Departamento de Química Orgánica I, Facultad de Ciencias Químicas, Universidad Complutense de Madrid, 28040 Madrid, Spain

Supporting Information

ABSTRACT: The effect of solvation by water molecules on the nucleophilicity of the superoxide anion, $O_2^{\bullet-}$, has been investigated in detail by mass spectrometric experiments and quantum chemical calculations, including direct dynamics trajectory calculations. Specifically, the S_N2 reactions of $O_2^{\bullet-}(H_2O)_n$ clusters (n = 0−5) with CH_3Cl and CH_3Br were studied. It was found that the reaction rate decreases when the number of water molecules in the cluster increases; furthermore, reaction with CH_3Br is in general faster than reaction with CH_3Cl for clusters of the same size. In addition, key transition-state geometries were identified and probed by Born−Oppenheimer molecular dynamics, showing how a water molecule may be transferred from the nucleophile to the leaving group during the reaction. The computational models are in good agreement with the experimental observations.

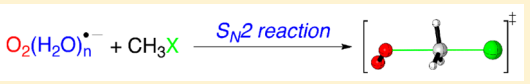

INTRODUCTION

It is well-known that nucleophilicity, and the ability of a molecule to donate an electron pair to a substrate and displace a leaving group during a bimolecular nucleophilic substitution reaction (S_N2), is strongly affected by solvent effects. For example, while the fluoride ion is a potent nucleophile in the isolated gas phase,[1−3] its reactivity in water solution is hampered by hydrogen bonds from the surrounding water molecules. It is therefore necessary to conduct nucleophilic substitution reactions under conditions where deactivation of the nucleophile by the solvent is minimized.[4−6]

The effect of gradual solvation on S_N2 reactivity was elegantly demonstrated by Bohme and co-workers already in 1981,[7,8] who observed a significant decrease in the reaction rates of water-clustered nucleophiles with increasing cluster size, e.g.,

$$OH^-(H_2O)_n + CH_3X \rightarrow X^-(H_2O)_m + CH_3OH + (n-m)H_2O \quad (n = 0, 1, 2, ...; X = Cl, Br) \qquad (1)$$

This effect was later reproduced in model calculations applying quantum chemical methods and transition-state theory.[9,10] Similar microsolvation effects have also been demonstrated for F^-, Cl^-, and HOO^-.[11,12]

The superoxide anion, $O_2^{\bullet-}$, is an essential intermediate in the cellular processes of electron transport, including the respiration chain and photosynthesis; it also plays a key role in the immune defense system of organisms.[13,14] As a reagent it did not find practical use in preparative organic chemistry until 1970 due to difficulties in finding suitable reaction conditions. In protic media, like water, disproportionation of $O_2^{\bullet-}$ to hydroxide and oxygen is fast (reaction 2), so an aprotic solvent has to be used.[15]

$$4O_2^{\bullet-} + 2H_2O \rightarrow 3O_2 + 4OH^- \qquad (2)$$

The first successful attempts of nucleophilic substitution reactions with superoxide involved its generation by electroreduction of solutions containing O_2.[16,17] Alkali metal superoxide salts are poorly soluble in typical aprotic solvents but can be used as a source of $O_2^{\bullet-}$ when a crown-ether is used as a cosolvent.[18,19] Recently, it was demonstrated that even transition-metal superoxide complexes may display nucleophilic reactivity.[20] It turns out that $O_2^{\bullet-}$ is a strong nucleophile with a clear preference for inversion of configuration at the central carbon atom during an S_N2 reaction, which makes it a versatile reagent for various enantiospecific substitution and addition reactions.[21−23] The properties of $O_2^{\bullet-}$ and its reactivity are issues of great concern in rechargeable LiO_2 battery technology.[24] Furthermore, the superoxide anion is relevant to aqueous environments as it is affecting the redox balance in water, being produced in the reaction between ozone and hydroxide anions and in reactions between various organic substances and hydroxyl radicals.[25,26] It has also been found that $O_2^{\bullet-}$ is produced by photoreduction in seawater[27] and in atmospheric droplets containing transition-metal ions.[28,29] It should also be mentioned that superoxide is effective in rapid degradation of halogenated aromatics to environmentally less harmful products[30,31] and may also be of some relevance for the effect of indoor air cleaning machines.[32]

In ambient air the average concentration of ions may amount to a few thousands per cm^3,[33,34] these are for the most part resulting from ionization by cosmic radiation and radioactive sources, including radon. The only major component of air with an appreciable electron affinity is O_2 (EA ≈ 0.45 eV),[35] indicating that superoxide is an anion of significant impact on atmospheric ion chemistry. It seems likely that it will be quickly

Received: March 23, 2015

DOI: 10.1021/acs.joc.5b00651
J. Org. Chem. XXXX, XXX, XXX−XXX

hydrated and thereby exist in the form of small $O_2^{\bullet-}(H_2O)_n$ clusters. The lifetime of anions in the troposphere is of the order of 10^3 s due to dissociative recombination with positive ions.[34,36−38] However, $O_2^{\bullet-}(H_2O)_n$ clusters are depleted in reactions with ozone, therefore affording $O_3^-(H_2O)_n$:[33]

$$O_2^{\bullet-}(H_2O)_n + O_3 \rightarrow O_3^{\bullet-}(H_2O)_{n-1} + O_2 + H_2O \quad (3)$$

$O_2^{\bullet-}(H_2O)_n$ clusters are also considered as an important precursor in various reactions involving nitrogen and sulfur oxidation, ultimately giving nitrate and nitrate/sulfate/water clusters as products.[39] The detailed mechanisms of some of these reactions are still unclear. In thunderstorms, ionization is enhanced, providing a significant contribution to terrestrial NO_x production and thereby nitrogen fixation, perhaps involving $O_2^{\bullet-}$ as an intermediate.[40]

On this basis it has become important to investigate the properties and reactivity of superoxide and superoxide/water clusters in the gas phase, both in order to learn about the atmospheric chemistry of the species and from a more fundamental point of view to understand how $O_2^{\bullet-}$ reactivity is moderated by hydration. In general agreement with the solution-phase behavior, the gas-phase reactivity of bare $O_2^{\bullet-}$ has been probed experimentally by mass spectrometry and is found to act as a nucleophile in substitution reactions with CH_3Cl, CH_3Br, various $CH_3O(CO)R$ esters, CF_3Cl, CF_3Br, CF_3I, $C_2H_2Cl_2$, C_2HCl_3, C_2H_3F, $C_2H_2F_2$, C_2HF_3, C_2F_4, and C_6F_6.[31,41−44] In other words, $O_2^{\bullet-}$ displays nucleophilic vinylic and aromatic substitution reactivity in addition to aliphatic S_N2 reactivity.

Water clusters containing the superoxide anion, $O_2^{\bullet-}(H_2O)_n$, can be formed rather conveniently using several mass spectrometric techniques,[45−48] and gas-phase exchange reactions have been observed with O_3, CO_2, NO, and SO_2.[33] The properties of $O_2^{\bullet-}(H_2O)_n$ clusters have been determined by thermochemical measurements,[45] IR spectroscopic signatures (Ar predissociation),[49] electron photodetachment characteristics,[50] and quantum chemical calculations.[51] All data support the idea that $O_2^{\bullet-}$ is well solvated by water molecules by hydrogen-bond donation and that the first solvation shell probably contains four water molecules.

To our knowledge there exists no previous study on S_N2 reactions of $O_2^{\bullet-}(H_2O)_n$ clusters. Here we present kinetic data on the reactions of such clusters with methyl chloride and methyl bromide. Besides studying the size effect, i.e., the effect the degree of hydration has on reactivity, it was of interest to investigate the effect of the leaving group and to examine the nature of the products. In the same manner as nucleophilicity is expected to decrease upon increased hydration, the ability of the leaving group to leave the substrate (nucleofugacity) is expected to increase. However, this would require water molecule transfer from the nucleophile to the leaving group during reaction. In order to help with the interpretation of the data, we have conducted quantum chemical calculations of the selected reaction profiles, including the identification of key intermediates and transition-state geometries. In addition, Born−Oppenheimer direct dynamics calculations were conducted to examine the product formation in detail, with particular emphasis on the possibility of water molecule transfer during the reaction.

RESULTS AND DISCUSSION

Reaction Products and Kinetics. The in vacuo reaction of $O_2^{\bullet-}(H_2O)_n$ with CH_3Cl and CH_3Br (n = 0−5) was studied at different center-of-mass (COM) collision energies using a mass spectrometer (see the Experimental Section). Although our experimental system allows for keeping alkyl halide pressure fairly constant during the experiment, absolute CH_3Cl and CH_3Br pressure calibration is difficult to obtain. For this reason, reaction rates are given relative to an internal normalization.

The data collected for the reactions of superoxide/water cluster anions with methyl chloride and methyl bromide are displayed in Figures 1 and 2, respectively. The figures show the rate coefficients of the two main reaction channels for the methyl halides CH_3X, where X = Cl or Br. The two reaction channels are the formation of possibly hydrated X^- (nucleophilic substitution):

$$O_2^{\bullet-}(H_2O)_n + CH_3X \rightarrow X^-(H_2O)_x + CH_3O_2^{\bullet}(H_2O)_{n-x-y} + yH_2O \quad (4)$$

and the CH_3X incorporation reaction:

$$O_2^{\bullet-}(H_2O)_n + CH_3X \rightarrow O_2^{\bullet-}(CH_3X)(H_2O)_{n-z} + zH_2O \quad (5)$$

In these experiments, the hydration of the halide in the nucleophilic substitution reaction (reaction 4) was limited to x = 0, 1; the rates given represent the combined intensity of these products (formation of $X^-(H_2O)$ by X^- capturing a water molecule from the background gas can be ruled out, as explained in the Experimental Section). Note that the exact nature of the neutral products in reaction 4, i.e., the number of H_2O molecules attached to $CH_3O_2^{\bullet}$, is not known from the experiments. Typically, the number of water molecules $n - x - y$ would depend upon the enthalpy of the S_N2 reaction as well as the collision energy. Likewise, the exact chemical nature of the molecules making up the product cluster-ion in reaction 5 is not known, although the number of water molecules evaporating from the cluster (z) during the reaction can be indicative. Results from quantum chemical calculations are of course enlightening in both cases.

As seen in Figure 1, the rate coefficient for the nucleophilic substitution reaction involving CH_3Cl decreases with increasing number of water molecules in the cluster, giving straight lines in

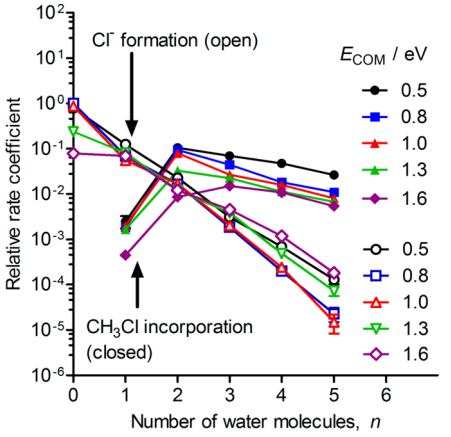

Figure 1. Relative rate coefficients for $O_2^{\bullet-}(H_2O)_n$ + CH_3Cl leading to Cl^- formation (nucleophilic substitution) and to CH_3Cl incorporation. The data are given for different COM collision energies and cluster sizes n and have been normalized to the Cl^- formation reaction of $O_2^{\bullet-}$ at 0.8 eV. Error bars represent one SD due to count statistics.

DOI: 10.1021/acs.joc.5b00651
J. Org. Chem. XXXX, XXX, XXX−XXX

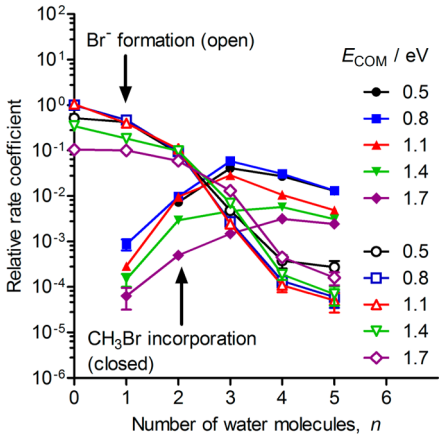

Figure 2. Relative rate coefficients for $O_2^{\bullet-}(H_2O)_n$ + CH_3Br leading to Br^- formation (nucleophilic substitution) and to CH_3Br incorporation. The data are given for different COM collision energies and cluster sizes n and have been normalized to the Br^- formation reaction of $O_2^{\bullet-}$ at 0.8 eV. Error bars represent one SD due to count statistics.

the semilogarithmic plots; in other words, the reaction rate decreases in an exponential fashion with increasing cluster size. This functional dependence is, however, most likely a coincidence. We also note that increasing the collision energy increases S_N2 reactivity for the more hydrated clusters, likely a consequence of the additional energy present in the reaction intermediate allowing for easier desolvation of the superoxide anion prior to the reaction. For the less hydrated clusters, higher collision energy instead gives lower S_N2 reactivity, which could result from the shrinking of the velocity-dependent induced dipole capture cross section.

In addition to the direct evidence for nucleophilic substitution, we also observe significant incorporation of CH_3Cl in the $O_2^{\bullet-}(H_2O)_n$ clusters. This process is accompanied by the loss of, typically, one or two water molecules and dominates for $n \geq 2$. The rate of this process is retarded by increasing the collision energy and more so for n = 2 than for the larger clusters.

Although, we are not able to conduct experiments at 0.00 eV COM collision energy—corresponding to approximately thermal conditions—with our experimental setup, we consider it correct to extrapolate the observed trends in reactivity with collision energy to this point, thereby clearly showing that the reactions occur spontaneously without the need of the infusion of external energy under thermal conditions.

The experimental results for CH_3Br, shown in Figure 2, display in broad terms the same trends as observed for CH_3Cl; however, there are important differences. For n = 0, 1, and 2 the substitution reaction products dominate, while CH_3Br incorporation dominates for $n \geq 3$. It is also clear that the decrease in reaction rate for Br^- formation decreases by only half an order of magnitude in going from n = 0 to 2, compared to CH_3Cl where the corresponding decrease is 2 orders of magnitude. Consequently, the crossover from substitution products to incorporation products occurs at a higher value of n for CH_3Br compared to CH_3Cl. In line with this we also note that the nucleophilic substitution reaction curve for CH_3Br is S-shaped compared to the essentially straight line for CH_3Cl.

As explained above, the data in Figures 1 and 2 are normalized internally to the S_N2 reaction of $O_2^{\bullet-}$ with CH_3Cl and CH_3Br, respectively. To compare the data of the two figures on a common scale of reference, one may take advantage of the relative rate coefficient for the two reactions:

$$O_2^{\bullet-} + CH_3Cl \rightarrow Cl^- + CH_3O_2^{\bullet} \quad (6)$$

$$O_2^{\bullet-} + CH_3Br \rightarrow Br^- + CH_3O_2^{\bullet} \quad (7)$$

which is known to be 1.00:1.76 (both reactions are estimated to occur close to collision frequency).[41]

As mentioned above, two products were observed in the nucleophilic substitution reactions: the naked halide anion or the monohydrated halide anion. The ratio of the former to the combined intensity of both is shown in Figure 3, for both halides.

For methyl chloride, Figure 3a, the ratio between the two products can be seen to vary with both cluster size and collision energy. In the case of n = 1, the signal intensities correspond to at least an 80% preference in forming the bare chloride anion compared to the singly hydrated one; although depending upon energy, it can be even higher. For the other cluster sizes, there is an approximately 3:1 advantage for the hydrated chloride anion at lower collision energies; however, this advantage decreases with increasing collision energy, especially for n = 2 which is dominated by formation of Cl^- at 1.6 eV COM collision energy. In contrast, the branching ratios for methyl bromide (Figure 3b) have the naked halide ion as the dominating product for all cluster sizes except n = 5.

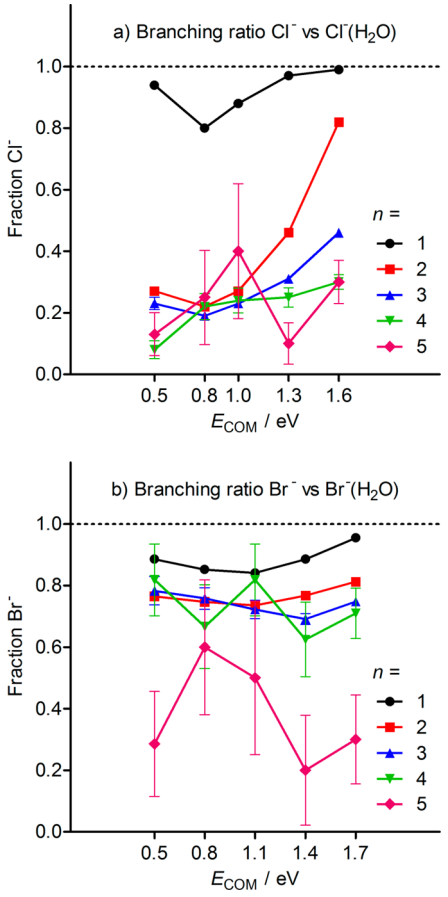

Figure 3. Branching ratio $X^-/(X^- + X^-(H_2O))$ for the nucleophilic substitution reactions of $O_2^{\bullet-}(H_2O)_n$ with CH_3X. X = Cl (top) and X = Br (bottom). Error bars represent one SD due to count statistics.

DOI: 10.1021/acs.joc.5b00651
J. Org. Chem. XXXX, XXX, XXX−XXX

Furthermore, the strong dependence on collision energy observed for the formation of Cl^- vs the formation of $Cl^-(H_2O)$ when n = 2, 3 is absent for all cluster sizes in the bromide case. This will be discussed further in the Reaction Dynamics section.

Reaction Energetics and Mechanisms. The potential energy diagrams—calculated at the DFT(B3LYP)/6-311+G(d,p) level—of the reactions of methyl chloride with superoxide, superoxide monohydrate, and superoxide dihydrate are displayed in Figure 4. The corresponding energy diagrams for methyl bromide reactions are displayed in Figure 5. For each step in the energy diagrams, only the lowest-energy structure is included, with the exception of the transition-state geometries.

The transition-state geometries for the methyl chloride reactions with $O_2^{\bullet-}(H_2O)_n$ can be found in Figures 6–8; bond lengths are indicated in the figures. The transition-state geometries for the methyl bromide reactions are not displayed, as they have the same general features as the corresponding methyl chloride ones. The bond lengths of the transition-state geometries for the methyl bromide case can be found in the Supporting Information Table S1 (atom numbers as indicated in Figures 7 and 8).

For calibration purposes, we have also used the OPBE functional because it has been proved to provide good accuracy in estimating the barriers of nucleophilic substitution

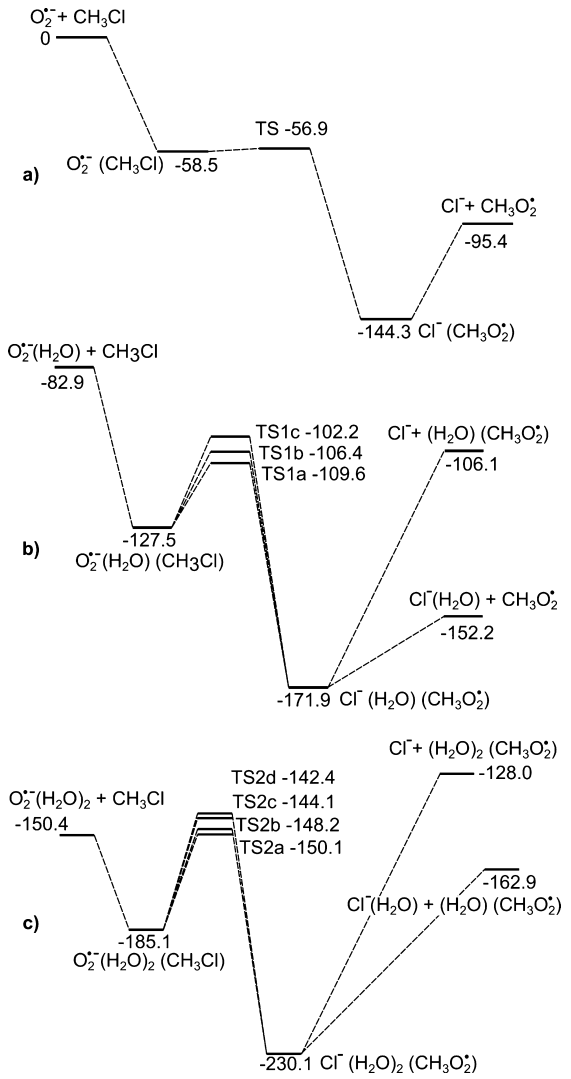

Figure 4. DFT(B3LYP)/6-311+G(d,p) potential energy diagram (including zero-point vibration energies) for the nucleophilic substitution reaction between $O_2^{\bullet-}(H_2O)_n$ and CH_3Cl. The relative energies are given in kJ mol^{-1}. Panel (a) n = 0, energies relative to separated $O_2^{\bullet-}$ + CH_3Cl; panel (b) n = 1, energies relative to separated $O_2^{\bullet-}$ + H_2O + CH_3Cl; and panel (c) n = 2, energies relative to separated $O_2^{\bullet-}$ + $2H_2O$ + CH_3Cl.

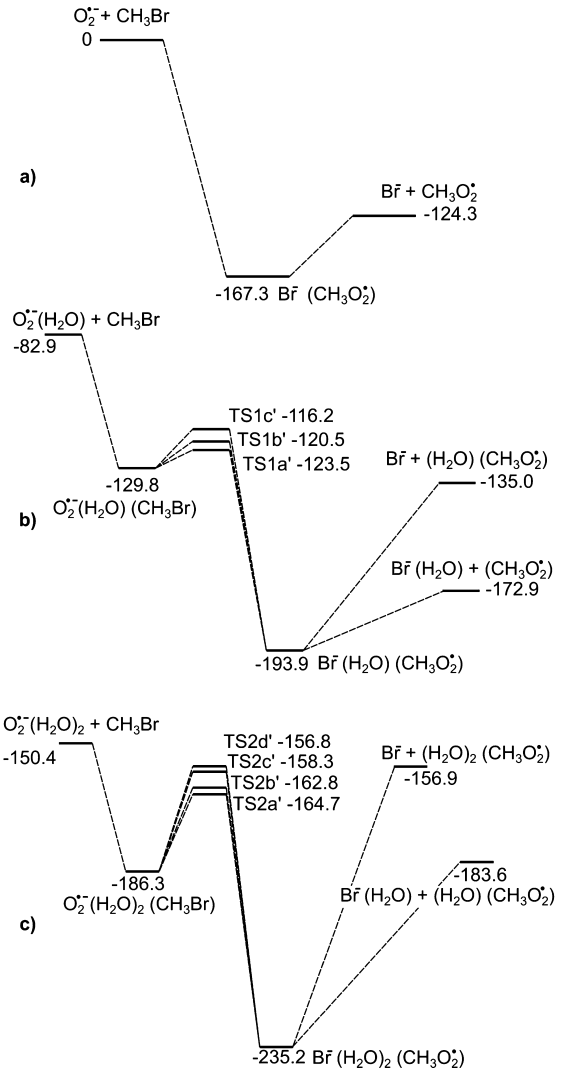

Figure 5. DFT(B3LYP)/6-311+G(d,p) potential energy diagram (including zero-point vibration energies) for the reaction between $O_2^{\bullet-}(H_2O)_n$ and CH_3Br. The relative energies are given in kJ mol^{-1}. Panel (a) n = 0, energies relative to separated $O_2^{\bullet-}$ + CH_3Br (no barrier with B3LYP); panel (b) n = 1, energies relative to separated $O_2^{\bullet-}$ + H_2O + CH_3Br; and panel (c) n = 2, energies relative to separated $O_2^{\bullet-}$ + $2H_2O$ + CH_3Br.

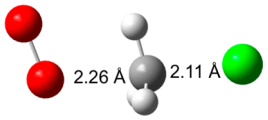

Figure 6. Fully optimized (DFT(B3LYP)/6-311+G(d,p) level) transition-state geometry (**TS**) of the central barrier for the substitution reaction between the superoxide anion and methyl chloride; see Figure 4a.

DOI: 10.1021/acs.joc.5b00651
J. Org. Chem. XXXX, XXX, XXX−XXX

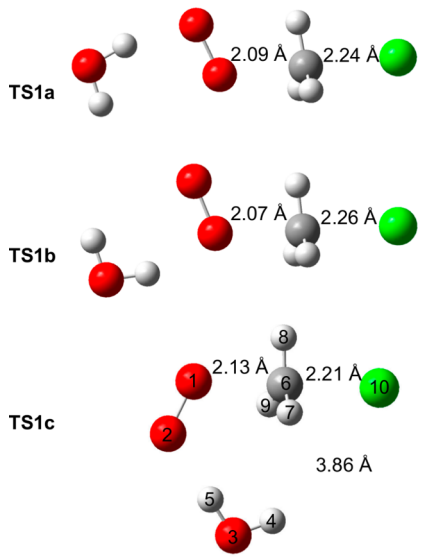

Figure 7. Fully optimized (DFT(B3LYP)/6-311+G(d,p) level) transition-state geometries, **TS1a**, **TS1b**, and **TS1c**, of the three central barriers for the substitution reaction between the monohydrated superoxide anion and methyl chloride; see Figure 4b.

reactions.[3,52−54] Our OPBE results (see Supporting Information Figure S1) concur quite well with the data (both computed energies and geometries) obtained at the B3LYP level, giving only slightly higher barriers, in agreement with general knowledge.[63]

For convenience, Table 1 shows the energy levels of the S_N2 reaction products (reaction 4) relative to the energy levels of the reactants, i.e., the data in Figures 4 and 5 with the energy of the reactant cluster set to zero. The energetics for the incorporation reaction, i.e., adding a methyl halide to the cluster without having the nucleophilic substitution reaction (reaction 5), can also be extracted from Figures 4 and 5 and are summarized in Table 2 (note that some values are unavailable for the CH_3Br case as the calculations using the B3LYP functional failed to find a $O_2^{\bullet-}(CH_3Br)$ intermediate).

Table 1. Energies (kJ mol^{-1}, computed at the DFT(B3LYP)/6-311+G(d,p) level) of Products Relative to Reactants for the Substitution Reactions

reaction	relative energy
$O_2^{\bullet-} + CH_3Cl \rightarrow Cl^- + CH_3O_2^{\bullet}$	−95.4
$O_2^{\bullet-}(H_2O) + CH_3Cl \rightarrow Cl^-(H_2O) + CH_3O_2^{\bullet}$	−69.3
$O_2^{\bullet-}(H_2O) + CH_3Cl \rightarrow Cl^- + (H_2O)(CH_3O_2^{\bullet})$	−23.2
$O_2^{\bullet-}(H_2O) + CH_3Cl \rightarrow Cl^- + CH_3O_2^{\bullet} + H_2O$	−12.5
$O_2^{\bullet-}(H_2O)_2 + CH_3Cl \rightarrow Cl^-(H_2O) + (CH_3O_2^{\bullet})(H_2O)$	−14.3
$O_2^{\bullet-}(H_2O)_2 + CH_3Cl \rightarrow Cl^-(H_2O) + CH_3O_2^{\bullet} + H_2O$	−3.6
$O_2^{\bullet-}(H_2O)_2 + CH_3Cl \rightarrow Cl^- + (H_2O)_2(CH_3O_2^{\bullet})$	+20.6
$O_2^{\bullet-}(H_2O)_2 + CH_3Cl \rightarrow Cl^- + (H_2O)(CH_3O_2^{\bullet}) + H_2O$	+42.5
$O_2^{\bullet-}(H_2O)_2 + CH_3Cl \rightarrow Cl^- + CH_3O_2^{\bullet} + 2H_2O$	+53.2
$O_2^{\bullet-} + CH_3Br \rightarrow Br^- + CH_3O_2^{\bullet}$	−124.3
$O_2^{\bullet-}(H_2O) + CH_3Br \rightarrow Br^-(H_2O) + CH_3O_2^{\bullet}$	−90.0
$O_2^{\bullet-}(H_2O) + CH_3Br \rightarrow Br^- + (H_2O)(CH_3O_2^{\bullet})$	−52.1
$O_2^{\bullet-}(H_2O) + CH_3Br \rightarrow Br^- + CH_3O_2^{\bullet} + H_2O$	−41.4
$O_2^{\bullet-}(H_2O)_2 + CH_3Br \rightarrow Br^-(H_2O) + (CH_3O_2^{\bullet})(H_2O)$	−35
$O_2^{\bullet-}(H_2O)_2 + CH_3Br \rightarrow Br^-(H_2O) + CH_3O_2^{\bullet} + H_2O$	−24.3
$O_2^{\bullet-}(H_2O)_2 + CH_3Br \rightarrow Br^- + (H_2O)_2(CH_3O_2^{\bullet})$	−8.3
$O_2^{\bullet-}(H_2O)_2 + CH_3Br \rightarrow Br^- + (H_2O)(CH_3O_2^{\bullet}) + H_2O$	+13.6
$O_2^{\bullet-}(H_2O)_2 + CH_3Br \rightarrow Br^- + CH_3O_2^{\bullet} + 2H_2O$	+24.3

Several features appear clear from the $O_2^{\bullet-}(H_2O)_n + CH_3Cl$ energy diagrams in Figure 4. First, the reaction exothermicity for the S_N2 reaction (reaction 4) decreases significantly with increasing cluster size, apparently an effect of the stronger hydration of the ionic $O_2^{\bullet-}$ compared to the neutral methylperoxyl radical; we also note that the reactions are more exothermic when the formed chloride ion is hydrated. Second, and directly related to this effect, it is seen that the efficient potential energy barrier increases from −57 kJ mol^{-1} for $n = 0$, via −27 kJ mol^{-1} for $n = 1$, to 0 kJ mol^{-1} for $n = 2$. If the computed energy values can be taken literally, and extrapolation is valid, this would indicate that the S_N2 barrier lies significantly above the energy of the reactants from $n = 3$ and onward. This of course implies that the S_N2 reactivity should decrease quickly with cluster size, which is in good agreement with the experimental observation. Also in agreement with this picture: it is seen from the experiments that the CH_3Cl incorporation reaction, which is likely to only have a small energy barrier, overhauls the S_N2 reaction already at $n = 2$.

In our calculations, the monohydrated superoxide anion starts from one conformer and splits into three possible transition-state geometries (Figure 7) upon its reaction with methyl chloride (of which one, **TS1c**, allows the formation of a hydrated chloride anion). In contrast, the dihydrated superoxide anion starts from three different cluster conformers (seen in the Supporting Information Figure S2), providing three different initial reactant complexes with methyl chloride. The reaction complexes follow the reaction path into four energetically close (within 6 kJ mol^{-1}) but structurally distinct local minima which then continue to four different transition-state geometries **TS2a**−**TS2d** (Figure 8). Out of these, the two transition-state geometries **TS2c** and **TS2d** are distinct, allowing the formation of a $Cl^-(H_2O)$ product, whereas the other two do not. This will be further discussed in the Reaction Dynamics section.

Now, turning our attention to the energy profiles obtained for methyl bromide (Figure 5, Table 1), we notice that the computed reaction energies for these reactions are considerably larger in magnitude (i.e., more negative) than those for methyl chloride, as expected from the relative C−X bond dissociation energies. In general agreement with the Hammond postulate,[55,56] this has the consequence that the reaction barriers for $n = 0$, 1, and 2 (absent for $n = 0$) are clearly lower for methyl bromide. We therefore better understand the experimental finding that the relative rates for nucleophilic substitution for

Table 2. Energies (kJ mol^{-1}, computed at the DFT(B3LYP)/6-311+G(d,p) level) of Products Relative to Reactants for the Incorporation Reactions

reaction	relative energy
$O_2^{\bullet-} + CH_3Cl \rightarrow O_2^{\bullet-}(CH_3Cl)$	−58.5
$O_2^{\bullet-}(H_2O) + CH_3Cl \rightarrow O_2^{\bullet-}(H_2O)(CH_3Cl)$	−44.6
$O_2^{\bullet-}(H_2O) + CH_3Cl \rightarrow O_2^{\bullet-}(CH_3Cl) + H_2O$	+24.4
$O_2^{\bullet-}(H_2O)_2 + CH_3Cl \rightarrow O_2^{\bullet-}(H_2O)_2(CH_3Cl)$	−34.7
$O_2^{\bullet-}(H_2O)_2 + CH_3Cl \rightarrow O_2^{\bullet-}(H_2O)(CH_3Cl) + H_2O$	+47.3
$O_2^{\bullet-}(H_2O)_2 + CH_3Cl \rightarrow O_2^{\bullet-}(CH_3Cl) + 2H_2O$	+91.9
$O_2^{\bullet-}(H_2O) + CH_3Br \rightarrow O_2^{\bullet-}(H_2O)(CH_3Br)$	−46.9
$O_2^{\bullet-}(H_2O)_2 + CH_3Br \rightarrow O_2^{\bullet-}(H_2O)_2(CH_3Br)$	−35.9
$O_2^{\bullet-}(H_2O)_2 + CH_3Br \rightarrow O_2^{\bullet-}(H_2O)(CH_3Br) + H_2O$	+56.5

DOI: 10.1021/acs.joc.5b00651
J. Org. Chem. XXXX, XXX, XXX−XXX

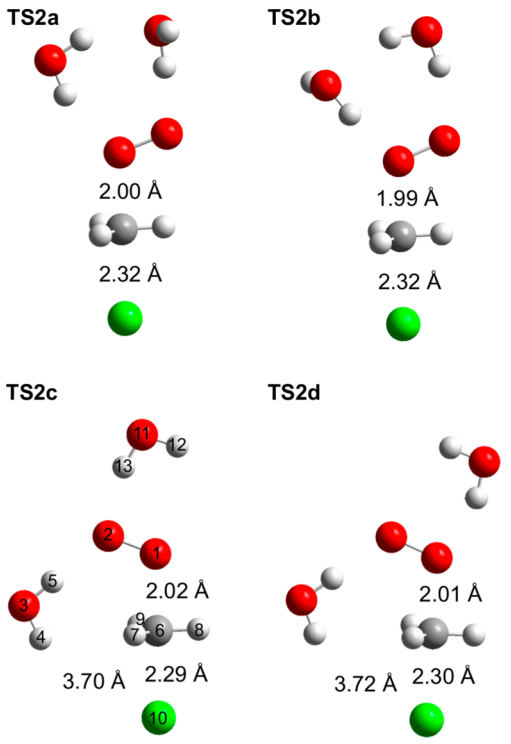

Figure 8. Fully optimized (DFT(B3LYP)/6-311+G(d,p) level) transition-state geometries, **TS2a**, **TS2b**, **TS2c**, and **TS2d**, of the four central barriers for the substitution reaction between the dihydrated superoxide anion and methyl chloride; see Figure 4c.

clusters in this size range is faster for CH_3Br than for CH_3Cl. Moreover, an effective potential energy barrier of −14 kJ mol^{-1} for n = 2 (compared to 0 kJ mol^{-1} for CH_3Cl) could indicate that the barrier for n = 3 is not much above zero in the CH_3Br case. This corresponds nicely with the crossover from a preference for nucleophilic substitution to a preference for alkyl halide inclusion occurring between n = 2 and 3 for CH_3Br (see Figure 2) and not between n = 1 and 2 as for CH_3Cl (see Figure 1).

As noted in the introduction, the ability of the leaving group to leave the substrate is expected to increase if a water transfer occurs from the nucleophile to the leaving group. This is indeed the case, as seen for the S_N2 products in Figures 4 and 5. However, the energy level of these products is actually higher (relative to the reactants and the preceding intermediate) for $O_2^{\bullet-}(H_2O)_2$ compared to $O_2^{\bullet-}(H_2O)$; this implies that the effect will give diminishing returns as hydration increases above n = 2.

Reaction Dynamics. It has already been mentioned that the rate coefficient for methyl halide inclusion decreases with increasing collision energy, while that of nucleophilic displacement decreases for small clusters and increases for larger clusters with increasing collision energy. A number of different effects need to be considered here. First, it can easily be understood from Langevin theory that the capture cross section between an ion and an induced dipole decreases with increasing relative velocity;[57−59] this effect should influence both types of reactions equally. For the S_N2 reaction this effect is—at least for larger clusters—countered by the possibility that more energy rich collisions will lead to easier desolvation of the nucleophile or lead to evaporation of H_2O before the S_N2 reaction; both cases facilitating easier access of the nucleophile to the methyl halide. However, for the incorporation reaction, there is no process that increases the likelihood of methyl halide being incorporated into the cluster that could counteract the shrinking of the cross section at higher collision energies. If anything, higher collision energy will likely mean a lower probability of incorporation even if a cluster−gas collision occurs.

The branching ratio for $O_2^{\bullet-}(H_2O)$ producing Cl^- as opposed to $Cl^-(H_2O)$ upon encountering CH_3Cl reveals a clear preference for the former in these experiments (Figure 3a). This can be understood from the relative energy levels in Table 1. As the energy level of the monohydrated product is −69.3 kJ mol^{-1} relative to the reactants, any formed monohydrated chloride ions will be rather hot. As they will be unable to thermalize under the current experimental conditions (high vacuum), a large fraction are likely to decompose to Cl^- + H_2O during the relevant experimental time frame, in general agreement with the experimental findings. A local maximum for the $Cl^-(H_2O)$ formation is observed at 0.8 eV in Figure 3a. This can be qualitatively understood by considering that further increasing the collision energy will produce hotter products, but it will also decrease the characteristic experimental time frame allowing hotter products to survive until detection. At intermediate collision energies the two factors will balance.

For $O_2^{\bullet-}(H_2O)_2$ only products involving the hydrated chloride are below the reactants in energy (Figure 4, Table 1); however, they are fairly close to the energy of the reactants and therefore we expect these products to survive until detection. If we take into account the contributions from the collision energy, 0.5−1.6 eV = 48−154 kJ mol^{-1} (COM), we will find also the Cl^- products to be within range. Thus, we should expect both $Cl^-(H_2O)$ and Cl^- at low collision energies, while we expect almost exclusively formation of Cl^- at higher collision energies. Again, this appears to be in good agreement with the experimental branching ratio (Figure 3a).

The case for $O_2^{\bullet-}(H_2O)$ + CH_3Br is essentially analogous to $O_2^{\bullet-}(H_2O)$ + CH_3Cl as outlined above: the exothermicity of the $Br^-(H_2O)$ formation (Table 1) leads to clusters that are sufficiently hot to decompose before detection in the instrument as seen in Figure 3b.

For $O_2^{\bullet-}(H_2O)_2$ + CH_3Br we find experimentally that we have a strong preference to form the naked ion for all collision energies. This is in contrast to the chlorine case, where we—at least at lower collision energies—favored the hydrated ion. One reason for this is likely that hydrated bromine products, $Br^-(H_2O)$ + $(H_2O)(CH_3O_2^{\bullet})$ and $Br^-(H_2O)$ + $CH_3O_2^{\bullet}$ + H_2O, are lower in energy compared to the reactants than the corresponding chlorine products by 20.7 kJ mol^{-1} (Table 1). Another factor is that, given the same reduced collision energy, the flight time of bromine products through the instrument is longer than the flight time of the corresponding chlorine products which allows more time for the hot products to fragment in the former case.

We will now turn our attention to the incorporation reactions. As some computational values are unavailable for the CH_3Br case, we will consider only the incorporation of methyl chloride here. In the experiments, the incorporation reaction $O_2^{\bullet-}(H_2O)$ + CH_3Cl only has one product, $O_2^{\bullet-}(CH_3Cl)$, regardless of collision energy; this is unsurprising given that the energy necessary to evaporate the water molecule (nominally 24.4 kJ mol^{-1}, Table 2) is available already at a collision energy of 0.5 eV (48 kJ mol^{-1}). It should be noted

DOI: 10.1021/acs.joc.5b00651
J. Org. Chem. XXXX, XXX, XXX−XXX

that the resulting cluster would still be rather hot and prone to fragmenting into $O_2^{\bullet-}$ + CH_3Cl, especially at higher collision energies (1.6 eV = 154 kJ mol^{-1}). This is in agreement with the low detection frequency of $O_2^{\bullet-}(CH_3Cl)$ in the experiments (the incorporation reaction for n = 1 in Figure 1), especially at 1.6 eV.

As seen in Figure 1, the incorporation reaction of $O_2^{\bullet-}(H_2O)_2$ + CH_3Cl has a comparably high rate coefficient, at least for lower collision energies. The reaction is found to produce both $O_2^{\bullet-}(H_2O)(CH_3Cl)$ + H_2O and $O_2^{\bullet-}(CH_3Cl)$ + $2H_2O$, with the branching ratios of 92:8 at 0.5 eV collision energy and 80:20 at 1.6 eV collision energy. Given the relative energies in Table 2, we would expect more of the latter product and less of the former at 1.6 eV; however, in absolute terms, $O_2^{\bullet-}(H_2O)(CH_3Cl)$ decreases in intensity by a factor 2.57, while $O_2^{\bullet-}(CH_3Cl)$ decreases by a factor 0.94, when going from 0.5 to 1.6 eV collision energy. It should be noted that there are several factors here that have not been taken into account, such as Doppler broadening of the collision energy due to the thermal motion of the gas,[60] the shorter residence time of the meta stable clusters at higher collision energies, and the decrease in the evaporation rate with each successive loss of H_2O.[61] While a more thorough analysis is possible, it is beyond the scope of this work.

All these considerations are essentially based on thermochemistry. In reality, the final outcome of an encounter between two reacting molecules is intimately linked to the detailed reaction dynamics of the collision. Furthermore, the observation of $Cl^-(H_2O)$ product formation in the reaction between $O_2^{\bullet-}(H_2O)$ and CH_3Cl means that the water molecule transfers from the nucleophile to the nucleofuge during reaction. The question then arises whether this occurs before, during, or after the nucleophilic displacement. From the energy landscape depicted in Figure 4b, we identify three mechanistically and energetically very similar routes to pass from the reactant to the product side for $O_2^{\bullet-}(H_2O)$ + CH_3Cl. Of these three, passage via the transition-state geometry denoted **TS1c** is different from the other two by having the water molecule pointing one of its hydrogen atoms toward the departing chloride ion (see Figure 7), although with a rather long (3.86 Å) and thereby weak O−H···Cl hydrogen bond. In order to probe the post-transition-state dynamics we ran a series of direct dynamics trajectory calculations (B3LYP/6-311+G(d,p)), starting at transition-state geometries **TS1a**, **TS1b**, and **TS1c**. Inspection of the animations of these trajectories shows that the water molecule indeed moves toward the departing chloride ion upon passage of the transition-state geometry **TS1c** but that the detailed dynamics (and inherently the energy deposition) depends on the initial conditions. Indeed, only half of the trajectories end up with the water molecule bonded to the chloride ion in a dynamically stable fashion, most of them (80%) doing so within the first 500 fs, the rest within 1 ps. For the other half of the trajectories the water molecule is liberated giving a bare Cl^- (Table 3). Figure 9a shows a plot of descriptive internuclear distances for one representative trajectory ending up to give $Cl^-(H_2O)$. The very weak O−H···Cl hydrogen bond within **TS1c** seems not to be decisive for the eventual formation of $Cl^-(H_2O)$, since it fluctuates much in length during the first stage of the trajectory after passing the transition-state geometry. Instead, it appears to be the advantageous position of this water molecule on the brink of the reaction center that makes it attractive to the Cl atom as the Cl atom develops more Cl^- character during the second part of the trajectory after passing the transition-state geometry.

Table 3. Branching Ratios for Cl^- and $Cl^-(H_2O)$ Resulting from Trajectory Calculations (B3LYP/6-311+G(d,p) level) for $O_2^{\bullet-}(H_2O)$ + CH_3Cl

transition-state geometry	no. of trajectories	$Cl^-(H_2O)$	Cl^-
TS1a	37	0%	100%
TS1b	47	0%	100%
TS1c	46	45%	55%

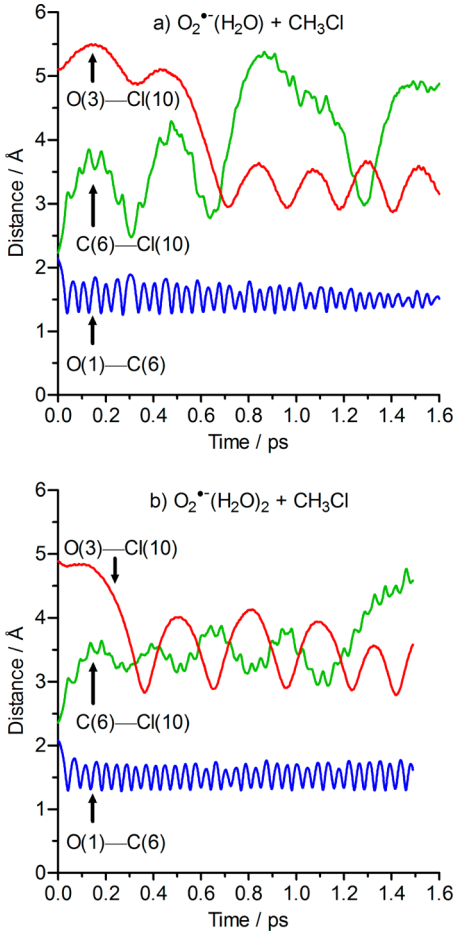

Figure 9. Typical direct dynamics (B3LYP/6-311+G(d,p)) trajectories (atomic distances as a function of time) for the reaction $O_2^{\bullet-}(H_2O)_n$ + CH_3Cl giving $Cl^-(H_2O)$. Panel (a) n = 1, starting from **TS1c**. Panel (b) n = 2, starting from **TS2c**. The red curve corresponds to the O(3)−Cl(10) distance (the distance between the water oxygen and chlorine), the blue curve corresponds to the O(1)−C(6) distance (the distance between the superoxide oxygen performing the nucleophilic attack and the carbon), and the green curve corresponds to the C(6)−Cl(10) distance (the distance between the superoxide oxygen performing the nucleophilic attack and the chlorine). The atom numbering can be seen in Figures 7 and 8.

A second set of trajectory calculations instead started from the separated reactant species. Unfortunately, the total integration time required for a statistically significant number of such trajectories is prohibitive; out of 91 trajectories, we observed the reaction passing to the products only 7 times, in each case with only Cl^- as final ionic product. In order to estimate the relative rates by which the three different transition-state geometries may be reached, we instead performed RRKM calculations in the microcanonical frame-

DOI: 10.1021/acs.joc.5b00651
J. Org. Chem. XXXX, XXX, XXX−XXX

work at an energy of +0.517 eV relative to the reactants (this corresponds to 0.5 eV nominal collision energy and average thermal contributions). The outcome of this calculation is k_1:k_2:k_3 = 2.39:3.37:1.0, corresponding to passing through the transition-state geometries **TS1a**, **TS1b**, and **TS1c**, respectively. In other words, crossing **TS1c** is predicted to occur for 14.8% of the reactive events. When we now correct for the result of the trajectory calculations in the sense that only 45% of trajectories that originate from **TS1c** give rise to $Cl^-(H_2O)$ (see Table 3), we obtain 6.7% only. This fits very well with experimental observation for the $O_2^{\bullet-}(H_2O)$ cluster at 0.5 eV nominal collision energy, which can be seen to be 6% in Figure 3a. Similarly, in the case of monohydrated methyl bromide, we performed 38 trajectory calculations starting from the transition-state geometries **TS1c′**. Out of these 50% give rise to the formation of $Br^-(H_2O)$. The RRKM calculations provide us with the ratio of k_1:k_2:k_3 = 2.02:1.42:1.0 for the relative reaction rates for passing the three transition-state geometries **TS1a′**, **TS1b′**, and **TS1c′**, respectively. Crossing the transition-state geometry **TS1c′** then occurs in 22.5% of the reactive events, which leads to the formation of $Br^-(H_2O)$ in 11.25% in total; also this is in good agreement with the experimental result of 11.5% in Figure 3b. It should be stressed at this point that the branching ratios thus calculated are rather crude estimates; as such, even though agreement with the experimental results is good this fact should not be given too high significance.

Given the approximate nature of these comparisons, the fact that the number of trajectories necessary to reach any amount of statistical certainty undoubtedly will be larger, and the fact that the calculations will be more demanding, we have opted to not extend this analysis to $O_2^{\bullet-}(H_2O)_2$ in full. However, we have performed some trajectory calculations for $O_2^{\bullet-}(H_2O)_2$ + CH_3Cl, now limiting ourselves to trajectories originating from **TS2c** and **TS2d**. These two transition-state geometries have one water molecule in a position similar to the water molecule in **TS1c** from the $O_2^{\bullet-}(H_2O)$ + CH_3Cl reaction, with the water donating a weak hydrogen bond to the chlorine atom. Figure 9b shows a typical trajectory giving rise to hydrated chloride as the ionic product. Also for these transition-state geometries we have an approximately 50:50 distribution between Cl^- and $Cl^-(H_2O)$ (see Table 4).

CONCLUSIONS

Here we have used joint experimental−computational methodology to gain more insight into the nucleophilic substitution reactions involving the superoxide anion, a molecular entity of relevance to biology and atmospheric science. The effect on the nucleophilicity of this species due to water molecules attached to it has been investigated in detail. It was found that for the reactions between superoxide/water cluster anions and CH_3Cl, the corresponding reaction rates decrease when the number of water molecules increases. Similar results have been found for the reaction involving CH_3Br instead of CH_3Cl. In nice agreement with these experimental findings, our density functional theory calculations clearly indicate that the attachment of water molecules to the superoxide anion is translated into higher S_N2 activation barriers, i.e., from a practically barrierless process for bare $O_2^{\bullet-}$ to significantly increasing barrier heights by the addition of one and two water molecules. The fact that we do not observe S_N2 reaction products for larger clusters does not rule out the possibility that in-cluster S_N2 reactions may occur at longer reaction times, since they remain invisible to the mass spectrometric experiments presented here. These results confirm the role of $O_2^{\bullet-}$ as a possible organic halide scavenger also when solvated by some water molecules. Although disproportionation of $O_2^{\bullet-}$ is known to occur in water solution, it seems not to be an issue in pure, small water clusters.

Table 4. Branching Ratios for Cl^- and $Cl^-(H_2O)$ Resulting from Trajectory Calculations (B3LYP/6-311+G(d,p) level) for $O_2^{\bullet-}(H_2O)_2$ + CH_3Cl

transition-state geometry	no. of trajectories	$Cl^-(H_2O)$	Cl^-
TS2c	21	52%	48%
TS2d	11	55%	45%

EXPERIMENTAL SECTION

The experiments were performed using a quadrupole time-of-flight mass spectrometer, which has been described in previous publications.[62−66] The instrument has been modified to allow for volatile and semivolatile gases to be injected into the collision cell by means of a stainless steel inlet system fitted with an ultrahigh-vacuum leak valve.

Cluster ions were produced by means of the electrospray ionization (ESI) unit fitted to the instrument. The ESI unit was operated at atmospheric pressure and room temperature, with nitrogen gas; water (HiPerSolv Chromanorm for HPLC, VWR BDH Prolabo) was fed through the electrospray capillary at a rate of 25 μL min^{-1}. A voltage of 3.0−3.5 kV was applied to the electrospray needle, leading to weak corona discharge at the needle tip and the formation of several types of anion−water clusters, e.g., $OH^-(H_2O)_n$, $HO_2^-(H_2O)_n$, and $O_2^{\bullet-}(H_2O)_n$. The resulting clusters were transferred into the high-vacuum part of the instrument, where the quadrupole mass filter—operating at better than unit resolution—allowed for transmission of a single $O_2^{\bullet-}(H_2O)_n$ cluster size based on the cluster's mass-to-charge ratio (m/z).

The cluster ions were introduced to the collision cell (length 16 cm, with hexapole ion guide) at a well-defined lab-frame kinetic energy. CH_3Cl (Aldrich 295507, 99.5%) or CH_3Br (Fluka 65950, purum ~99%) was introduced into the collision cell via the ultrahigh-vacuum leak valve. The methyl halide pressure was adjusted to limit double collisions while maintaining a sufficiently high collision frequency to avoid problems with signal-to-noise ratios and count statistics (error bars representing one SD due to count statistics are included for all data points in Figures 1−3, although they are for most data points too small to be discernible). This resulted in a pressure of 3−5 × 10^{-5} mbar, at which approximately 10% of the reactant ions react with the methyl halide. Detection of products and unreacted clusters was done by the time-of-flight unit, fitted with a chevron-type microchannel plate (MCP) detector. The voltages applied to the MCP detector were calibrated before the experiment so that the isotopic pattern of $Na^+(NaCl)_n$ clusters were faithfully reproduced; this ensured that no bias toward larger or smaller mass spectrum peaks existed. The sodium chloride clusters were produced from a 30 mM NaCl(aq) solution (NaCl: 99.5%) and using a higher temperature (100 °C) on the ESI source.

In order to determine variations in the collision gas pressure as the experiments proceeded, reference measurements were conducted at regular intervals, using the $O_2^{\bullet-}(H_2O)_2$ ion at 0.8 eV (COM) collision energy. The reference measurements allowed us to correct for slow variations in collision gas pressure that occurred. Background measurements were performed; these were identical to the experimental measurements in all aspects except that methyl halide gas was not introduced to the collision cell. In addition to the parent ion, the only ions observed in the background measurements correspond to loss of H_2O from the former due to metastable decay or collisions with background gas. The background pressure in the collision cell was approximately 6 × 10^{-6} mbar. This background gas originates from the ESI unit and, therefore, consists of mainly nitrogen

DOI: 10.1021/acs.joc.5b00651
J. Org. Chem. XXXX, XXX, XXX−XXX

and up to 2.3% water vapor (based on the vapor pressure of H_2O at atmospheric pressure and 295.15 K);[67] consequently, the partial pressure of H_2O in the collision cell is likely no more than 1.4×10^{-7} mbar (also during the measurements with methyl halides). The possible influence on the experimental results by water vapor in the background gas needs to be addressed; specifically if the monohydrated halide ion can be formed by H_2O capture from the surrounding gas. However, given the 2 orders of magnitude difference in pressure between the methyl halides and H_2O in the collision cell it is very unlikely that any cluster ion or formed reaction product will collide with a H_2O molecule in the collision cell (as the partial pressure of the methyl halides only results in approximately 10% of the cluster ions reacting). As such, any formation of $X^-(H_2O)$ by addition of H_2O to X^- after the cluster-methyl halide reaction should be insignificant compared to the formation of $X^-(H_2O)$ in the cluster-methyl halide reaction itself. This is further supported by the fact that the observed occurrence of the monohydrated halide anion contra the naked halide anion is dependent upon cluster size (Figure 3).

QUANTUM CHEMICAL CALCULATIONS

Quantum chemical calculations were carried out using the program system Gaussian 09.[68] All structures (reactants, transition structures, and products) were characterized by complete geometry optimization using the hybrid density functional B3LYP,[69] in conjunction with the 6-311+G(d,p) basis set.[70] Additional calculations were performed using the OPBE functional,[71,72] in conjunction with the 6-311++G(d,p) basis set. This latter method has been shown to provide accurate estimates on S_N2 barrier heights.[52,73] In each case the character of a stationary point (transition-state geometry or minimum energy structure) was identified from analysis of the eigenvalues of the molecular Hessian and by visual inspection. Relative energies were corrected by including unscaled zero-point vibrational energies (ZPVE) obtained from the harmonic frequencies. Furthermore, for each transition-state geometry that was localized, the reaction coordinate was followed to verify that the minimum potential reaction path leads to the expected reactant and product minima.

In order to examine the product formation, Born–Oppenheimer direct dynamics calculations with DFT-(B3LYP)/6-311+G(dp) were performed starting from the respective transition-state geometry and also from the reactant species. The initial vibrational states corresponding to 300 K were constructed using quasi-classical normal mode sampling.[74,75] The initial rotational energy is chosen from thermal distribution assuming symmetric top.

In the case of $O_2^{\bullet-}(H_2O)$ with methyl chloride we calculated a total of 130 trajectories when starting from the three optimized transition-state geometries; going up to 1.6 ps with a time step of 0.16 fs. When instead starting from the reactant species, using 6 different input orientations, we calculated 91 trajectories up to 3.5 ps with a time step of 0.175 fs. Out of 91 trajectories starting from the reactants we observed the reaction passing to the products in only 7 cases. None of them show the formation of the $Cl^-(H_2O)$ ionic product. The reaction with methyl bromide was examined by calculating 38 trajectories starting from the transition state **TS1c′** (from which the formation of the $Br^-(H_2O)$ ionic product is possible).

For $O_2^{\bullet-}(H_2O)_2$ we calculated 32 trajectories starting from the two transition-state geometries that are most likely involved in the formation of the $Cl^-(H_2O)$ ionic product. In this case the trajectories were 1.5 ps long with a time step of 0.15 fs.

ASSOCIATED CONTENT

Supporting Information

Bond lengths of the transition-state geometries for the substitution reaction of $O_2^{\bullet-}(H_2O)$ and $O_2^{\bullet-}(H_2O)_2$ with CH_3Br and results for the OPBE calculations as well as the stable conformers of the superoxide water cluster. Coordinates and absolute energies for all calculated geometries are given. The Supporting Information is available free of charge on the ACS Publications website at DOI: 10.1021/acs.joc.5b00651.

AUTHOR INFORMATION

Corresponding Authors

*E-mail: mauritz.ryding@kjemi.uio.no

*E-mail: einar.uggerud@kjemi.uio.no

Notes

The authors declare no competing financial interest.

ACKNOWLEDGMENTS

This work was supported by the Norwegian Research Council by the Grants no. 205512/F20, Nanosolvation in Hydrogen-Bonded Clusters (no. 179568/V30) to the Centre of Theoretical and Computational Chemistry through their Centre of Excellence program, and the Norwegian Supercomputing Program (NOTUR) through a grant of computer time (no. NN4654K). The Spanish MINECO-FEDER (grants CTQ2013-44303-P and CTQ2014-51912-REDC) and NILS Project (002-ABEL-CM-2013) are gratefully acknowledged.

REFERENCES

(1) Depuy, C. H.; Gronert, S.; Mullin, A.; Bierbaum, V. M. *J. Am. Chem. Soc.* **1990**, *112*, 8650–8655.
(2) Uggerud, E. *J. Phys. Org. Chem.* **2006**, *19*, 461–466.
(3) Fernández, I.; Frenking, G.; Uggerud, E. *Chem.—Eur. J.* **2009**, *15*, 2166–2175.
(4) Gerstenberger, M. R. C.; Haas, A. *Angew. Chem., Int. Ed.* **1981**, *20*, 647–667.
(5) Smith, M. D.; March, J. *Advanced Organic Chemistry*; 5th ed.; Wiley-Interscience: New York, 2001.
(6) Kim, D. W.; Jeong, H. J.; Litn, S. T.; Sohn, M. H.; Katzenellenbogen, J. A.; Chi, D. Y. *J. Org. Chem.* **2008**, *73*, 957–962.
(7) Bohme, D. K.; Mackay, G. I. *J. Am. Chem. Soc.* **1981**, *103*, 978–979.
(8) Bohme, D. K.; Raksit, A. B. *J. Am. Chem. Soc.* **1984**, *106*, 3447–3452.
(9) Ohta, K.; Morokuma, K. *J. Phys. Chem.* **1985**, *89*, 5845–5849.
(10) Tucker, S. C.; Truhlar, D. G. *J. Am. Chem. Soc.* **1990**, *112*, 3347–3361.
(11) Bohme, D. K.; Raksit, A. B. *Can. J. Chem.* **1985**, *63*, 3007–3011.
(12) Thomsen, D. L.; Reece, J. N.; Nichols, C. M.; Hammerum, S.; Bierbaum, V. M. *J. Am. Chem. Soc.* **2013**, *135*, 15508–15514.
(13) Afanas'ev, I. B. *Superoxide Ion: Chemistry and Biological Implications*; 1st ed.; CRC Press: Boca Raton, 1989; Vol *I*.
(14) Afanas'ev, I. B. *Superoxide Ion: Chemistry and Biological Implications*; 1st ed.; CRC Press: Boca Raton, 1991; Vol *II*.
(15) Cotton, F. A.; Wilkinson, G. *Advanced Inorganic Chemistry*; 5th ed.; Wiley-Interscience: New York, 1988.
(16) Merritt, M. V.; Sawyer, D. T. *J. Org. Chem.* **1970**, *35*, 2157–2159.
(17) Dietz, R.; Forno, A. E. J.; Larcombe, B. E.; Peover, M. E. *J. Chem. Soc. B* **1970**, 816–820.
(18) Valentine, J. S.; Curtis, A. B. *J. Am. Chem. Soc.* **1975**, *97*, 224–226.
(19) Sanfilippo, J.; Chern, C. I.; Valentine, J. S. *J. Org. Chem.* **1975**, *40*, 1678–1680.

DOI: 10.1021/acs.joc.5b00651
J. Org. Chem. XXXX, XXX, XXX–XXX

(20) Pirovano, P.; Magherusan, A. M.; McGlynn, C.; Ure, A.; Lynes, A.; McDonald, A. R. *Angew. Chem., Int. Ed.* **2014**, *53*, 5946−5950.
(21) Corey, E. J.; Nicolaou, K. C.; Shibasaki, M.; Machida, Y.; Shiner, C. S. *Tetrahedron Lett.* **1975**, 3183−3186.
(22) Danen, W. C.; Warner, R. J.; Arudi, R. L. In *Organic Free Radicals; ACS Symposium Series*; Pryor, W. A., Ed.; American Chemical Society: Washington, DC, 1978; Vol. *69*, pp 244−257.
(23) Sawyer, D. T.; Valentine, J. S. *Acc. Chem. Res.* **1981**, *14*, 393−400.
(24) Bryantsev, V. S.; Giordani, V.; Walker, W.; Blanco, M.; Zecevic, S.; Sasaki, K.; Uddin, J.; Addison, D.; Chase, G. V. *J. Phys. Chem. A* **2011**, *115*, 12399−12409.
(25) Staehelin, J.; Hoigne, J. *Environ. Sci. Technol.* **1985**, *19*, 1206−1213.
(26) Tomiyasu, H.; Fukutomi, H.; Gordon, G. *Inorg. Chem.* **1985**, *24*, 2962−2966.
(27) Voelker, B. M.; Sedlak, D. L. *Mar. Chem.* **1995**, *50*, 93−102.
(28) Weschler, C. J.; Mandich, M. L.; Graedel, T. E. *J. Geophys. Res. Atmos.* **1986**, *91*, 5189−5204.
(29) Graedel, T. E.; Mandich, M. L.; Weschler, C. J. *J. Geophys. Res. Atmos.* **1986**, *91*, 5205−5221.
(30) Sugimoto, H.; Matsumoto, S.; Sawyer, D. T. *Environ. Sci. Technol.* **1988**, *22*, 1182−1186.
(31) Sugimoto, H.; Matsumoto, S.; Sawyer, D. T.; Kanofsky, J. R.; Chowdhury, A. K.; Wilkins, C. L. *J. Am. Chem. Soc.* **1988**, *110*, 5193−5195.
(32) Daniels, S. L. *IEEE Trans. Plasma Sci.* **2002**, *30*, 1471−1481.
(33) Fahey, D. W.; Bohringer, H.; Fehsenfeld, F. C.; Ferguson, E. E. *J. Chem. Phys.* **1982**, *76*, 1799−1805.
(34) Eisele, F. L. *J. Geophys. Res. Atmos.* **1989**, *94*, 2183−2196.
(35) Bartmess, J. E. Negative Ion Energetics Data. In *NIST Chemistry WebBook, NIST Standard Reference Database*; Linstrom, P. J., Mallard, W. G., Eds.; National Institute of Standards and Technology: Gaithersburg, MD, 2015; Vol. *69*. http://webbook.nist.gov (accessed February 12, 2015).
(36) Mohnen, V. A. *J. Geophys. Res.* **1970**, *75*, 1717−1721.
(37) Bates, D. R. *Planet. Space Sci.* **1982**, *30*, 1275−1282.
(38) Beig, G.; Walters, S.; Brasseur, G. *J. Geophys. Res. Atmos.* **1993**, *98*, 12775−12781.
(39) Smith, D.; Spanel, P. *Mass. Spectrom. Rev.* **1995**, *14*, 255−278.
(40) Lorenz, R. D. In *Planetary Atmospheric Electricity*; Leblanc, F., Aplin, K. L., Yair, Y., Harrison, R. G., Lebreton, J. P., Blanc, M., Eds.; Springer-Verlag: New York, 2008; pp 287−296.
(41) Mcdonald, R. N.; Chowdhury, A. K. *J. Am. Chem. Soc.* **1985**, *107*, 4123−4128.
(42) Morris, R. A. *J. Chem. Phys.* **1992**, *97*, 2372−2381.
(43) Simpson, M. J. Ion-molecule reaction mass spectrometry and vacuum-ultraviolet negative photoion spectroscopy. *Ph.D. Thesis*, University of Birmingham, Birmingham, West Midlands, U.K., 2010.
(44) Kennedy, R. A.; Mayhew, C. A.; Peverall, R.; Watts, P. *Phys. Chem. Chem. Phys.* **2000**, *2*, 3145−3153.
(45) Arshadi, M.; Kebarle, P. *J. Phys. Chem.* **1970**, *74*, 1483−1485.
(46) Fehsenfeld, F. C.; Ferguson, E. E. *J. Chem. Phys.* **1974**, *61*, 3181−3193.
(47) Cabane, M.; Playe, P. *J. Aerosol Sci.* **1980**, *11*, 475−482.
(48) Yang, X.; Castleman, A. W. *J. Phys. Chem.* **1990**, *94*, 8500−8502.
(49) Weber, J. M.; Kelley, J. A.; Nielsen, S. B.; Ayotte, P.; Johnson, M. A. *Science* **2000**, *287*, 2461−2463.
(50) Luong, A. K.; Clements, T. G.; Resat, M. S.; Continetti, R. E. *J. Chem. Phys.* **2001**, *114*, 3449−3455.
(51) Lee, H. M.; Kim, K. S. *Mol. Phys.* **2002**, *100*, 875−879.
(52) Swart, M.; Solà, M.; Bickelhaupt, F. M. *J. Comput. Chem.* **2007**, *28*, 1551−1560.
(53) Fernández, I.; Frenking, G.; Uggerud, E. *J. Org. Chem.* **2010**, *75*, 2971−2980.
(54) Fernández, I.; Bickelhaupt, F. M.; Uggerud, E. *J. Org. Chem.* **2013**, *78*, 8574−8584.
(55) Hammond, G. S. *J. Am. Chem. Soc.* **1955**, *77*, 334−338.
(56) Pross, A. *Theoretical and Physical Principles of Organic Reactivity*; Wiley: New York, 1995.
(57) Langevin, P. *Ann. Chim. Phys.* **1905**, *5*, 245−288.
(58) Gioumousis, G.; Stevenson, D. P. *J. Chem. Phys.* **1958**, *29*, 294−299.
(59) Ridge, D. P. In *Structure/Reactivity and Thermochemistry of Ions*; Ausloos, P., Lias, S. G., Eds.; D. Reidel Publishing Company: Dordrecht, Netherlands, 1987; pp 1−14.
(60) Ervin, K. M.; Armentrout, P. B. *J. Chem. Phys.* **1985**, *83*, 166−189.
(61) Naher, U.; Hansen, K. *J. Chem. Phys.* **1994**, *101*, 5367−5371.
(62) Andersson, P. U.; Ryding, M. J.; Sekiguchi, O.; Uggerud, E. *Phys. Chem. Chem. Phys.* **2008**, *10*, 6127−6134.
(63) Zatula, A. S.; Andersson, P. U.; Ryding, M. J.; Uggerud, E. *Phys. Chem. Chem. Phys.* **2011**, *13*, 13287−13294.
(64) Ryding, M. J.; Zatula, A. S.; Andersson, P. U.; Uggerud, E. *Phys. Chem. Chem. Phys.* **2011**, *13*, 1356−1367.
(65) Ryding, M. J.; Jonsson, A. M.; Zatula, A. S.; Andersson, P. U.; Uggerud, E. *Atmos. Chem. Phys.* **2012**, *12*, 2809−2822.
(66) Ryding, M. J.; Ruusuvuori, K.; Andersson, P. U.; Zatula, A. S.; McGrath, M. J.; Kurtén, T.; Ortega, I. K.; Vehkamäki, H.; Uggerud, E. *J. Phys. Chem. A* **2012**, *116*, 4902−4908.
(67) Haar, L.; Gallagher, J. S.; Kell, G. S. In *CRC Handbook of Chemistry and Physics, internet version 2006*; 86th ed.; Lide, D. R., Ed.; Taylor and Francis: Boca Raton, FL, 2006; pp 6/8−6/9.
(68) Frisch, M. J.; Trucks, G. W.; Schlegel, H. B.; Scuseria, G. E.; Robb, M. A.; Cheeseman, J. R.; Scalmani, G.; Barone, V.; Mennucci, B.; Petersson, G. A.; Nakatsuji, H.; Caricato, M.; Li, X.; Hratchian, H. P.; Izmaylov, A. F.; Bloino, J.; Zheng, G.; Sonnenberg, J. L.; Hada, M.; Ehara, M.; Toyota, K.; Fukuda, R.; Hasegawa, J.; Ishida, M.; Nakajima, T.; Honda, Y.; Kitao, O.; Nakai, H.; Vreven, T.; Montgomery, J. A., Jr.; Peralta, J. E.; Ogliaro, F.; Bearpark, M.; Heyd, J. J.; Brothers, E.; Kudin, K. N.; Staroverov, V. N.; Kobayashi, R.; Normand, J.; Raghavachari, K.; Rendell, A.; Burant, J. C.; Iyengar, S. S.; Tomasi, J.; Cossi, M.; Rega, N.; Millam, J. M.; Klene, M.; Knox, J. E.; Cross, J. B.; Bakken, V.; Adamo, C.; Jaramillo, J.; Gomperts, R.; Stratmann, R. E.; Yazyev, O.; Austin, A. J.; Cammi, R.; Pomelli, C.; Ochterski, J. W.Martin, R. L.; Morokuma, K.; Zakrzewski, V. G.; Voth, G. A.; Salvador, P.; Dannenberg, J. J.; Dapprich, S.; Daniels, A. D.; Farkas, O.; Foresman, J. B.; Ortiz, J. V.; Cioslowski, J.; Fox, D. J. *Gaussian 09*, Rev. B.01; Gaussian, Inc.: Wallingford, CT, 2009.
(69) Becke, A. D. *J. Chem. Phys.* **1993**, *98*, 5648−5652.
(70) Curtiss, L. A.; Redfern, P. C.; Raghavachari, K. *J. Chem. Phys.* **2007**, *126*, 084108.
(71) Handy, N. C.; Cohen, A. J. *Mol. Phys.* **2001**, *99*, 403−412.
(72) Perdew, J. P.; Burke, K.; Ernzerhof, M. *Phys. Rev. Lett.* **1996**, *77*, 3865−3868.
(73) Swart, M.; Ehlers, A. W.; Lammertsma, K. *Mol. Phys.* **2004**, *102*, 2467−2474.
(74) Hase, W. L.; Buckowski, D. G. *Chem. Phys. Lett.* **1980**, *74*, 284−287.
(75) Hu, X. C.; Hase, W. L.; Pirraglia, T. *J. Comput. Chem.* **1991**, *12*, 1014−1024.

DOI: 10.1021/acs.joc.5b00651
J. Org. Chem. XXXX, XXX, XXX−XXX